Two-size moment Eulerian multi-fluid method describing the statistical trajectory crossing: modeling and numerical scheme

Matthieu Boileau, Julien Lagarde, Valentin Dupif, Frédérique Laurent, Marc Massot

Two-size moment Eulerian multi-fluid method describing the statistical trajectory crossing: modeling and numerical scheme

Matthieu Boileau[1], Julien Lagarde[2], Valentin Dupif[2,3,4], Frédérique Laurent[2,3] and Marc Massot[2,3,4*]

[1] *IRMA, CNRS-Unistra, UMR CNRS 7501*
Université de Strasbourg, 7 rue René Descartes, 67084 Strasbourg
matthieu.boileau@math.unistra.fr

[2] *Laboratoire EM2C, CNRS, CentraleSupélec, Université Paris-Saclay*
Grande Voie des Vignes, 92295 Châtenay-Malabry cedex, France
frederique.laurent@centralesupelec.fr, marc.massot@centralesupelec.fr

[3] *Fédération de Mathématiques de l'Ecole Centrale Paris, FR CNRS 3487, France*
Grande Voie des Vignes, 92295 Châtenay-Malabry cedex, France

[4] *Fundamental and applied Energetics Department*
ONERA Chemin de la Hunière Palaiseau FRANCE
valentin.dupif@onera.fr

Abstract

High fidelity modeling and simulation of turbulent dispersed two-phase flows is still a major challenge for many applications. Eulerian approaches are well suited for high performance computations of such flows. Recently, hybrid Eulerian methods that combine the multi-fluid approach - where the size is discretized - and the moment method were developed. On the one hand, in order to capture efficiently the size-polydispersion, two size moments were used on each interval of the size discretization (Two Size Moment method). On the other hand, the Anisotropic Gaussian (AG) velocity closure has been introduced as a relevant model to describe velocity dispersion occurring when the particles from the disperse phase have a significant inertia compared to the time scales of the flow, leading to particle trajectory crossings. The purpose of this contribution is to develop a model able to describe size and velocity dispersion, coupling the two-size moment Eulerian multi-fluid method and the anisotropic velocity closure. Adapted numerical schemes based on a relaxation method are provided. This new model (AG-TSM) is then evaluated on various test cases relevant to rocket propulsion and two-phase combustion.

Keywords: polydisperse spray, two-size moment Multi-Fluid model, moment method, particle trajectory crossing, relaxation scheme

1. Introduction

Two-phase flows constituted of a gaseous phase carrying a disperse condensed phase play a key role in many industrial and scientific applications like spray combustion in Diesel engines or aeronautical combustion chambers or internal flow dynamic of solid rocket motors where heterogeneous energetic materials are used. The resulting spray, composed of droplets of various sizes, can interact with the turbulent gaseous phase. To be able to predict the dynamic of these droplets, the description of this size polydispersion is necessary. Moreover, this can lead to trajectory crossings (Particle Trajectory Crossing - PTC), even between droplets of the same size (homo-PTC) if their inertia is high enough compared to the carrier flow time scales. Taking into account these two characteristics at a reasonable cost is a challenging task.

The spray is here described in a statistical sense using a kinetic approach: the Number Density Function (NDF) is considered and is solution of the Williams-Boltzmann equation [16]. As an alternative to Lagrangian Monte-Carlo methods, which are usually costly when aiming a good statistical convergence, and difficult to parallelize, Eulerian methods are developed. The main issues for this type of methods come 1) from its ability to take into account both the size and velocity polydispersion induced by both the large size spectrum and droplet trajectory crossing and also 2) from the development of adapted numerical schemes allowing to preserve the realizability of the moments (they have to stay moments of a positive measure).

On the one hand, an efficient hybrid method between the sectional and moment methods was introduced by Laurent et al. [10], improving the models developed in [8, 9]. It is able to describe accurately the size polydispersion in the context of moderately dense evaporating sprays through a discretization along the droplet size variable, the use of several moments in each size interval called section (two size moments additionally to the velocity moments of order one) and realizable and accurate numerical schemes for the transport, evaporation and coalescence. However, the underlying monokinetic assumption, considering that droplets of the same size has the same velocity, reaches its limits for inertial particles subject to homo-PTC. On the other hand, an anisotropic closure, inspired from theory of rarefied gas [11], were used in a second order velocity moment model, considering a size monodisperse spray [15]. It is the minimal closure able to predict PTC through moment methods [12, 13]. Moreover, a new generation of numerical methods based on relaxation schemes was developed in [2], which are able to handle these kinds of equations, and also to cope in a robust manner with the link both with zones without any velocity polydispersion and with vacuum area.

These three ingredients are put together here in order to obtain a model describing both size and velocity dispersion and develop adapted numerical schemes. The contribution is organized as follows: Section 2 is dedicated to the derivation of this hybrid model from the Williams-Boltzmann equation. Then, in Section 3, a realizable numerical strategy is presented for the resolution of the corresponding system of equations. Finally, in Section 4, the new model is evaluated on a 0D-test case for the order

* This work was supported by a grant from the French National Research Agency and the FRAE: NEXTFLAME project **(ANR-13-BS09-0023-01)**

of convergence and on a 2D-test case for the capacity to mimic evaporation and trajectory crossings at the same time.

2. Eulerian modeling of polydisperse sprays

Here, we first give the kinetic model describing a dilute evaporating spray and then the derivation of the hybrid method in two steps: the first one leading to equations on velocity moments at fixed size, using the anisotropic Gaussian closure, and the second step introducing the size discretization and moments on each section. The properties of the induced model are finally given.

2.1. Kinetic model

The spray can be described by its Number Density Function (NDF) $f(t,\boldsymbol{x},S,\boldsymbol{u})$, where $f(t,\boldsymbol{x},S,\boldsymbol{u})\mathrm{d}\boldsymbol{x}\mathrm{d}\boldsymbol{u}\mathrm{d}S$ denotes the average number of droplets (in a statistical sense) at time t, in a volume of size $\mathrm{d}\boldsymbol{x}$ around a space location $\boldsymbol{x}$, with a velocity in a $\mathrm{d}\boldsymbol{u}$-neighborhood of $\boldsymbol{u}$ and with a surface in a $\mathrm{d}S$-neighborhood of S. For the sake of simplicity and for the purpose of this paper, only the simple evaporation d^2 law is considered in such a way that the unsteady heating of the droplets does not need to be modeled. We refer to [8, 14] for a consideration of heating. When considering dilute inertial evaporating sprays, the evolution of this NDF is described by the following Boltzmann-type equation [16]:

$$\partial_t f + \partial_{\boldsymbol{x}}\cdot(\boldsymbol{u}\,f) + \partial_{\boldsymbol{u}}\cdot(F\,f) - \partial_S(K\,f) = 0, \tag{1}$$

where the evaporation rate K is a non-negative constant and the drag force $\boldsymbol{F}$ is described by the Stokes law $\boldsymbol{F} = \dfrac{\boldsymbol{u}_g - \boldsymbol{u}}{\tau_p(S)}$, with $\boldsymbol{u}_g(t,\boldsymbol{x})$ the gas velocity, $\tau_p(S) = \dfrac{\rho_l S}{18\pi\mu_g} \equiv \mathcal{A}S$ the relaxation time of the droplet velocity, ρ_l the liquid droplet material density, assumed constant, and $\mu_g(t,\boldsymbol{x})$ the gas dynamic viscosity. It would have been too costly to solve this equation directly through a full discretization. Then, only moments of first orders are considered.

2.2. Semi-kinetic model: Anisotropic Gaussian (AG) closure

Let us first consider the following velocity moments of order 0, 1 and 2, conditioned by size:

$$n(t,\boldsymbol{x},S) = \iint_{\mathbb{R}^d} f(t,\boldsymbol{x},S,\boldsymbol{u})\mathrm{d}\boldsymbol{u}. \tag{2}$$

$$n(t,\boldsymbol{x},S)\boldsymbol{u}_d(t,\boldsymbol{x},S) = \iint_{\mathbb{R}^d} \boldsymbol{u}\,f(t,\boldsymbol{x},S,\boldsymbol{u})\mathrm{d}\boldsymbol{u}. \tag{3}$$

$$n(t,\boldsymbol{x},S)\boldsymbol{E}(t,\boldsymbol{x},S) = \frac{1}{2}\iint_{\mathbb{R}^d} \boldsymbol{u}\otimes\boldsymbol{u}\,f(t,\boldsymbol{x},S,\boldsymbol{u})\mathrm{d}\boldsymbol{u}, \tag{4}$$

where d is the dimension of the physical space. The tensor $\boldsymbol{\Sigma}(t,\boldsymbol{x},S)$ is also introduced in such a way that $\boldsymbol{E} = \frac{1}{2}(\boldsymbol{u}_d\otimes\boldsymbol{u}_d + \boldsymbol{\Sigma})$. Since the conservation equations on the second order moments need information on the third order moments, these are modeled thanks to the assumption of a multi-variate Gaussian distribution in velocity [15, 13]:

$$f(t,\boldsymbol{x},S,\boldsymbol{u}) = n(t,\boldsymbol{x},S)G_{\boldsymbol{\Sigma}(t,\boldsymbol{x},S)}(\boldsymbol{u}-\boldsymbol{u}_d(t,\boldsymbol{x},S)), \tag{5}$$

where $G_{\boldsymbol{\Sigma}}(\boldsymbol{u})$ is a centered Gaussian density function of covariance matrix $\boldsymbol{\Sigma}$. The equations on the moments then read:

$$\partial_t n + \partial_{\boldsymbol{x}}\cdot(n\boldsymbol{u}_d) = \partial_S(Kn), \tag{6}$$

$$\partial_t(n\boldsymbol{u}_d) + \partial_{\boldsymbol{x}}\cdot(n(\boldsymbol{u}_d\otimes\boldsymbol{u}_d+\boldsymbol{\Sigma})) = \partial_S(Kn\boldsymbol{u}_d) + \frac{n}{\tau_p}(\boldsymbol{u}_g-\boldsymbol{u}_d),$$

$$\partial_t(n\boldsymbol{E}) + \partial_{\boldsymbol{x}}\cdot(n(\boldsymbol{E}+\boldsymbol{\Sigma})\vee\boldsymbol{u}_d) = \partial_S(Kn\boldsymbol{E}) + \frac{n}{\tau_p}(\boldsymbol{u}_g\vee\boldsymbol{u}_d-2\boldsymbol{E}),$$

where $\vee$ denotes the symmetric tensor outer product [11].

2.3. Hybrid model: AG-TSM

We consider the discretization $0 = S_0 < \cdots < S_N = S_{max}$ of the size interval $[0, S_{max}[$ and the following size-velocity moments of the NDF in the section k corresponding to $[S_{k-1}, S_k]$, skipping the $(t,\boldsymbol{x})$ dependence in the notations:

$$\begin{pmatrix} n_k \\ m_k \end{pmatrix} = \int_{S_{k-1}}^{S_k} \begin{pmatrix} 1 \\ \frac{\rho_l}{6\sqrt{\pi}}S^{3/2} \end{pmatrix} n(S)\mathrm{d}S, \tag{7}$$

$$m_k\boldsymbol{u}_k = \int_{S_{k-1}}^{S_k} \frac{\rho_l}{6\sqrt{\pi}}S^{3/2}n(S)\boldsymbol{u}_d(S)\mathrm{d}S, \tag{8}$$

$$m_k\boldsymbol{E}_k = \int_{S_{k-1}}^{S_k} \frac{\rho_l}{6\sqrt{\pi}}S^{3/2}n(S)\boldsymbol{E}(S)\mathrm{d}S. \tag{9}$$

Moreover, $\boldsymbol{\Sigma}_k$ is also defined by: $\boldsymbol{E}_k = \frac{1}{2}(\boldsymbol{u}_k\otimes\boldsymbol{u}_k + \boldsymbol{\Sigma}_k)$

To close the equations on these moments, the NDF is reconstructed from them. It means that the functions $n(S)$, $\boldsymbol{u}_d(S)$ and $\boldsymbol{\Sigma}(S)$ from (5) are presumed in each section k: $\boldsymbol{u}_d(S)$ and $\boldsymbol{\Sigma}(S)$ are assumed to be constant, equal to $\boldsymbol{u}_k$ and $\boldsymbol{\Sigma}_k$, and an affine by part reconstruction $\kappa_k(S)$ is used for $n(S)$, which was shown to be accurate and stable [10]. For this last function, three types of reconstruction are used, depending of the value of m_k/n_k. They are represented in Figure 1. Since two pure size moments, n_k and m_k are used in each section, the method is called TSM (two size moments), whereas it were called OSM (one size moment) when only m_k was used with a constant reconstruction in the section.

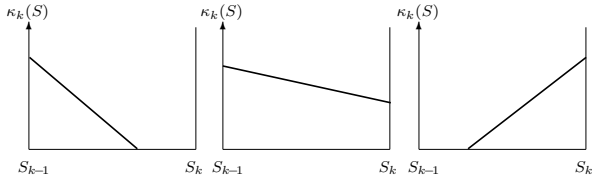

Figure 1: The three types of affine reconstructions.

With this presumed NDF, the equations are written:

$$\begin{aligned}
&\partial_t n_k + \partial_{\boldsymbol{x}}\cdot(n_k\boldsymbol{u}_d) = \mathcal{N}^{(k+\frac{1}{2})} - \mathcal{N}^{(k-\frac{1}{2})},\\
&\partial_t m_k + \partial_{\boldsymbol{x}}\cdot(m_k\boldsymbol{u}_d) = \mathcal{F}^{(k+\frac{1}{2})} - \mathcal{F}^{(k-\frac{1}{2})} - \mathcal{M}^{(k)},\\
&\partial_t(m_k\boldsymbol{u}_k) + \partial_{\boldsymbol{x}}\cdot(m_k(\boldsymbol{u}_k\otimes\boldsymbol{u}_k+\boldsymbol{\Sigma}_k)) = \frac{m_k}{\tau_k}(\boldsymbol{u}_g-\boldsymbol{u}_k)\\
&\quad + \mathcal{F}^{(k+\frac{1}{2})}\boldsymbol{u}_{k+1} - \mathcal{F}^{(k-\frac{1}{2})}\boldsymbol{u}_k - \mathcal{M}^{(k)}\boldsymbol{u}_k,\\
&\partial_t(m_k\boldsymbol{E}_k) + \partial_{\boldsymbol{x}}\cdot(m_k(\boldsymbol{E}_k+\boldsymbol{\Sigma}_k)\vee\boldsymbol{u}_k) = \frac{m_k}{\tau_k}(\boldsymbol{u}_g\vee\boldsymbol{u}_k-2\boldsymbol{E}_k)\\
&\quad + \mathcal{F}^{(k+\frac{1}{2})}\boldsymbol{E}_{k+1} - \mathcal{F}^{(k-\frac{1}{2})}\boldsymbol{E}_k - \mathcal{M}^{(k)}\boldsymbol{E}_k,
\end{aligned} \tag{10}$$

with $\tau_k = \mathcal{A}S_k^{moy}$ and

$$S_k^{moy} = \frac{\int_{S_{k-1}}^{S_k} S^{3/2}\kappa_k(S)\mathrm{d}S}{\int_{S_{k-1}}^{S_k} S^{1/2}\kappa_k(S)\mathrm{d}S}, \quad \mathcal{N}^{(k-\frac{1}{2})} = K\,\kappa_k(S_{k-1}), \tag{11}$$

$$\mathcal{F}^{(k-\frac{1}{2})} = K\,\frac{S^{3/2}}{6\sqrt{\pi}}\kappa_k(S_{k-1}), \quad \mathcal{M}^{(k)} = \int_{S_{k-1}}^{S_k}\frac{S^{1/2}}{4\sqrt{\pi}}K\kappa_k(S)\mathrm{d}S.$$

2.4. Model properties

To be moments of a positive NDF, our variables have to satisfy the following constraints: $\boldsymbol{\Sigma}_k$ has to be definite positive and

$$\frac{\rho_l}{6\sqrt{\pi}}S_{k-1}n_k < m_k < \frac{\rho_l}{6\sqrt{\pi}}S_k n_k \;\text{ or }\; (n_k,m_k) = (0,0). \tag{12}$$

The numerical scheme used to solve the equations then shall be designed in order to intrinsically preserve these realizability conditions and thus provide robustness without a posteriori corrections.

Moreover, the system is hyperbolic thanks to the use of the anisotropic Gaussian closure [15].

3. Numerical schemes

The scheme designed here benefits from the realizable ones developed in [10] in the monokinetic context and in [2] in the monodisperse context. For that, a Strang splitting strategy is used. The operators corresponding to transport in one side and to evaporation and drag in another side are then solved separately and alternatively with realizable schemes, presented in what follows.

3.1. Evaporation and drag

The operator corresponding to evaporation and drag leads to one ODE system per spatial cell:

$$\begin{aligned}
\partial_t n_k =& \mathcal{N}^{(k+\frac{1}{2})} - \mathcal{N}^{(k-\frac{1}{2})},\\
\partial_t m_k =& \mathcal{F}^{(k+\frac{1}{2})} - \mathcal{F}^{(k-\frac{1}{2})} - \mathcal{M}^{(k)},\\
\partial_t (m_k \boldsymbol{u}_k) =& \mathcal{F}^{(k+\frac{1}{2})}\boldsymbol{u}_{k+1} - \mathcal{F}^{(k-\frac{1}{2})}\boldsymbol{u}_k - \mathcal{M}^{(k)}\boldsymbol{u}_k\\
&+\frac{m_k}{\tau_k}(\boldsymbol{u}_g - \boldsymbol{u}_k),\\
\partial_t (m_k \boldsymbol{E}_k) =& \mathcal{F}^{(k+\frac{1}{2})}\boldsymbol{E}_{k+1} - \mathcal{F}^{(k-\frac{1}{2})}\boldsymbol{E}_k - \mathcal{M}^{(k)}\boldsymbol{E}_k\\
&+\frac{m_k}{\tau_k}(\boldsymbol{u}_g \vee \boldsymbol{u}_k - 2\boldsymbol{E}_k).
\end{aligned} \tag{13}$$

For its resolution, the Quadrature Kinetic Scheme (QKS) developed in [10] is adapted to take into account the additional variables. It can be seen as a Gauss quadrature technique to approximate the solution of the kinetic scheme, which uses the analytical solution at the kinetic level. Practically, three steps are involved: from an approximation n_k^n, m_k^n, $m_k^n \boldsymbol{u}_k^n$ and $m_k^n \boldsymbol{E}_k^n = \frac{1}{2} m_k^n \left(\boldsymbol{u}_k^n \otimes \boldsymbol{u}_k^n + \boldsymbol{\Sigma}_k^n\right)$ of the moments at time t^n

1) the NDF is reconstructed in each section k, thus defining the function $\kappa_k^n(S)$ from the n_k^n and m_k^n. Using the change of variable $R = \sqrt{S}$, the quadrature weights (w_1, w_2) and abscissas $\left(\sqrt{s_1^0}, \sqrt{s_2^0}\right)$ of the measure $2R\kappa_k^n(R^2)\mathbb{1}_{]S_{k-1}+K\Delta t, S_k[}(R^2)\mathrm{d}R$ and the quadrature weights $(\tilde{w}_1, \tilde{w}_2)$ and abscissas $\left(\sqrt{\tilde{s}_1}, \sqrt{\tilde{s}_2}\right)$ of the measure $2R\kappa_{k+1}^n(R^2)\mathbb{1}_{]S_k, S_k+K\Delta t[}(R^2)\mathrm{d}R$ are computed, with analytical formulas of [7] from the first four moments of such measures.

2) Then, one makes evolve the quadrature point characteristics, thus defining, for $i = 1, 2$,

$$\begin{aligned}
&s_i(t) = s_i^0 - Kt, && \tilde{s}_i(t) = \tilde{s}_i^0 - Kt,\\
&\boldsymbol{\sigma}_i(t) = \left(1 - \frac{Kt}{s_i^0}\right)^{\frac{2}{\mathcal{A}K}} \boldsymbol{\Sigma}_k^n, && \tilde{\boldsymbol{\sigma}}_i(t) = \left(1 - \frac{Kt}{\tilde{s}_i^0}\right)^{\frac{2}{\mathcal{A}K}} \boldsymbol{\Sigma}_{k+1}^n,
\end{aligned} \tag{14}$$

and solving the following systems, for $i = 1, 2$, during Δt:

$$\begin{cases} \mathrm{d}_t \boldsymbol{v}_i(t) = \dfrac{\boldsymbol{u}_g(t) - \boldsymbol{v}_i(t)}{\mathcal{A} s_i(t)}, \\ \boldsymbol{v}_i(0) = \boldsymbol{u}_k^n. \end{cases} \qquad \begin{cases} \mathrm{d}_t \tilde{\boldsymbol{v}}_i(t) = \dfrac{\boldsymbol{u}_g(t) - \tilde{\boldsymbol{v}}_i(t)}{\mathcal{A} \tilde{s}_i(t)}, \\ \tilde{\boldsymbol{v}}_i(0) = \boldsymbol{u}_{k+1}^n. \end{cases}$$

3) Finally, the new values of the moments are given by:

$$\begin{aligned}
n_k^{n+1} &= \sum_{i=1}^{2} w_i + \sum_{i=1}^{2} \tilde{w}_i,\\
m_k^{n+1} &= \frac{\rho_l}{6\sqrt{\pi}} \left(\sum_{i=1}^{2} w_i s_i (\Delta t)^{\frac{3}{2}} + \sum_{i=1}^{2} \tilde{w}_i \tilde{s}_i (\Delta t)^{\frac{3}{2}} \right),\\
m_k^{n+1} \boldsymbol{u}_k^{n+1} &= \frac{\rho_l}{6\sqrt{\pi}} \left(\sum_{i=1}^{2} w_i s_i (\Delta t)^{\frac{3}{2}} \boldsymbol{v}_i(\Delta t) \right.\\
&\qquad \left. + \sum_{i=1}^{2} \tilde{w}_i \tilde{s}_i (\Delta t)^{\frac{3}{2}} \tilde{\boldsymbol{v}}_i(\Delta t) \right),
\end{aligned}$$

$$\begin{aligned}
m_k^{n+1} \boldsymbol{E}_k^{n+1} =& \frac{\rho_l}{12\sqrt{\pi}} \left(\sum_{i=1}^{2} w_i s_i (\Delta t)^{\frac{3}{2}} \left[\boldsymbol{v}_i(\Delta t) \otimes \boldsymbol{v}_i(\Delta t) + \boldsymbol{\sigma}_i(\Delta t)\right] \right.\\
&\left. + \sum_{i=1}^{2} \tilde{w}_i \tilde{s}_i (\Delta t)^{\frac{3}{2}} \left(\tilde{\boldsymbol{v}}_i(\Delta t) \otimes \tilde{\boldsymbol{v}}_i(\Delta t) + \tilde{\boldsymbol{\sigma}}_i(\Delta t)\right) \right).
\end{aligned}$$

Let us remark that for a constant gas velocity, an analytical solution can be given for $\boldsymbol{v}_i(t)$ and $\tilde{\boldsymbol{v}}_i(t)$.

The obtained moment set is then necessarily realizable, as soon as the evaporation CFL-like number $\max_k \frac{K\Delta t}{S_k - S_{k-1}}$ is smaller than one.

3.2. Transport

The transport operator reads:

$$\begin{aligned}
&\partial_t (m_k \mu_k) + \partial_{\boldsymbol{x}} \cdot (m_k \mu_k \boldsymbol{u}_d) = 0,\\
&\partial_t m_k + \partial_{\boldsymbol{x}} \cdot (m_k \boldsymbol{u}_d) = 0,\\
&\partial_t (m_k \boldsymbol{u}_k) + \partial_{\boldsymbol{x}} \cdot (m_k (\boldsymbol{u}_k \otimes \boldsymbol{u}_k + \boldsymbol{\Sigma}_k)) = 0,\\
&\partial_t (m_k \boldsymbol{E}_k) + \partial_{\boldsymbol{x}} \cdot (m_k (\boldsymbol{E}_k + \boldsymbol{\Sigma}_k) \vee \boldsymbol{u}_k) = 0,
\end{aligned} \tag{15}$$

where we introduced $\mu_k = \frac{n_k}{m_k}$ which has to live in $\left]\frac{6\sqrt{\pi}}{\rho_l S_k^{3/2}}, \frac{6\sqrt{\pi}}{\rho_l S_{k-1}^{3/2}}\right[$. This condition will be ensured if the maximum principle on this variable is preserved by the numerical scheme.

First, a method of line is used, solving alternatively the operators corresponding to each direction. Here we only describe the scheme corresponding to the first direction, which is an adaptation to the anisotropic model of the scheme developed in [2]. A pressure relaxation scheme is used: only the nonlinearity associated to the pressure tensor is relaxed. Similarly to [1, 3, 4, 5], we introduce the following non linear first order system with singular perturbation:

$$\begin{aligned}
&\partial_t (m_k \mu_k) + \partial_1 (m_k \mu_k u_{k,1}) = 0,\\
&\partial_t m_k + \partial_1 (m_k u_{k,1}) = 0,\\
&\partial_t (m_k u_{k,1}) + \partial_1 (m_k u_{k,1}^2 + \Pi_{11}) = 0,\\
&\partial_t (m_k u_{k,2}) + \partial_1 (m_k u_{k,1} u_{k,2} + \Pi_{12}) = 0,\\
&\partial_t (m_k E_{k,11}) + \partial_1 (m_k E_{k,11} u_{k,1} + \Pi_{11} u_{k,1}) = 0,\\
&\partial_t (m_k E_{k,12}) + \partial_1 \left(m_k E_{k,12} u_{k,1} + \frac{1}{2}(\Pi_{12} u_{k,1} + \Pi_{11} u_{k,2})\right) = 0,\\
&\partial_t (m_k E_{k,22}) + \partial_1 (m_k E_{k,22} u_{k,1} + \Pi_{12} u_{k,2}) = 0,\\
&\partial_t \Pi + u_{k,1} \partial_1 \Pi + \frac{a^2}{m_k} \partial_1 u_{k,1} = \lambda (m_k \boldsymbol{\Sigma}_k - \Pi),
\end{aligned} \tag{16}$$

where the parameter λ is supposed to go to infinity, in such a way that the relaxation pressure Π tends to $m_k \boldsymbol{\Sigma}_k$, at least formally. For the stability of the relaxation procedure, the parameter a is chosen such that $a > m_k \sqrt{3\Sigma_{k,11}}$. The system admits the following three eigenvalues: $u_{k,1} \pm a/m_k$ with a second-order multiplicity and $u_{k,1}$, with a sixth-order multiplicity. These eigenvalues are associated with linearly degenerate characteristic fields.

The proposed numerical procedure is made in two steps [1, 2, 3, 4, 5]: first, the convective part of the pressure relaxation model (i.e. (16) for $\lambda = 0$) is solved using a Godunov method based on the exact Riemann solution, which can be explicitly

solved here, similarly to what is done in [2]. Then, the right-hand side of (16) is solved in the asymptotic regime $\lambda \to \infty$, meaning that Π is set to be equal to $m_k \mathbf{\Sigma}_k$. Let us remark that, like in [2], the parameter a is taken nonconstant, advected at the velocity $u_{k,1}$. The choice for this parameter is the same here, using $c = \sqrt{3\Sigma_{k,11}}$ for the sound speed, $u_{k,1}$ for the velocity and $m_k \Sigma_{k,11}$ for the pressure (still only considering the first direction). The obtained numerical scheme is realizable.

4. Result

4.1. Verification on a homogeneous test case

A fictive case is designed for the verification of the evaporation and drag scheme. A homogeneous test case is then considered, then skipping the $\boldsymbol{x}$ dependence: a polydisperse spray is considered with an initial 2D anisotropic Gaussian velocity distribution depending on size. It experiences drag and evaporation. The gas velocity is assumed constant: $u_{g,1} = 4\,m.s^{-1}$ in the first direction and $u_{g,2} = 2\,m.s^{-1}$ in the second one. The drag force is characterized by the coefficient $1/\mathcal{A} = 9.680385.10^{-7}\,m^2.s^{-1}$, the evaporation rate is $K = 1.99.10^{-7}\,m^2.s^{-1}$ and the liquid density is $\rho_l = 634.239\,kg.m^{-3}$. Finally, the initial distribution is defined for a size S from 0 to $S_{\max} = 11310\,\mu m^2$ (corresponding to a radius equal to $30\mu m$) in such a way that for $s \in [0,1]$:

$$f_0(sS_{\max}, u) = \Phi(s) G_{\Sigma(s)}\left(u - \overline{u}(s)\right), \tag{17}$$

with G_Σ the centered Gaussian density function of covariance matrix Σ. The spray mean velocity is an increasing function of the surface equal to the gas velocity at $S = 0$ (non-inertial droplets):

$$\overline{\boldsymbol{u}}(s) - \boldsymbol{u}_g = \psi(s)\,\delta\boldsymbol{u}, \qquad \psi(s) = s(2-s), \tag{18}$$

with $\delta u_1 = 1\,m.s^{-1}$, $\delta u_2 = 2\,m.s^{-1}$. In the same way, the covariance matrix components depend on size and are zero at $S = 0$:

$$\Sigma(s) = \sigma_0 \mathbf{A} \psi(s), \qquad \mathbf{A} = \begin{pmatrix} 1 & 0 \\ 0 & 2 \end{pmatrix}, \tag{19}$$

with $\sigma_0 = 1\,m^2.s^{-2}$. Finally, the normalized initial size distribution is given by the following regular function (see Fig. 2):

$$\Phi(s) = \phi_0\,(1+8s)\,(1-s)^2 \exp\left(0.001\left(1 - \frac{1}{(1-s)^2}\right)\right). \tag{20}$$

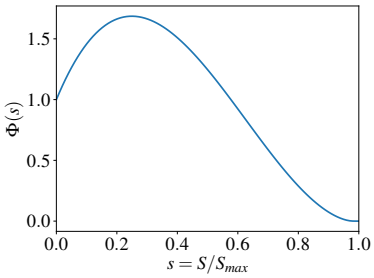

Figure 2: Initial normalized size distribution.

The analytical solution of this homogeneous problem reads:

$$f(t,S,u) = \left(1 + \frac{Kt}{S}\right)^{\frac{2}{\mathcal{A}K}} \Phi\left(\frac{S+Kt}{S_{\max}}\right) \tag{21}$$
$$G_{\Sigma\left(\frac{S+Kt}{S_{\max}}\right)}\left(\boldsymbol{u}_g + (\boldsymbol{u}-\boldsymbol{u}_g)\left(1+\frac{Kt}{S}\right)^{\frac{1}{\mathcal{A}K}} - \overline{\boldsymbol{u}}\left(\frac{S+Kt}{S_{\max}}\right)\right),$$

which is still a Gaussian distribution in velocity, in such a way that the model can capture it. Let us remark that even if there is no correlation between the velocities in the two directions, such kind of correlation appears globally for the spray due to its size polydispersion and size-dependent velocity distributions.

Thus, the size discretization and the numerical scheme for evaporation and drag are verified in this case compatible with the Gaussian assumption for the velocity. Simulations are done with the TSM and OSM models from $t = 0$ to $t = t_{\max} = 0.06\,s$. Three kinds of discretizations are considered, with 3, 10 and 100 equidistributed sections and the evaporation CFL like number is fixed to 0.2. The maximum values of the errors on the global variables $\sum_k n_k^n$, $\sum_k m_k^n$, $\sum_k m_k^n \boldsymbol{u}_k^n$, $\sum_k m_k^n \boldsymbol{E}_k^n$ are presented in table 1, normalized respectively by $\sum_k n_k^0$, $\sum_k m_k^0$, $\sum_k m_k^0 \|\boldsymbol{u}_g\|$, $\frac{1}{2}\sum_k m_k^0 \|\boldsymbol{u}_g\|^2$.

Table 1: Normalized maximum values of the errors on the global variables as a function of the number of sections N in the homogeneous test case for the TSM model and compared to the OSM model for $N = 100$.

N	$\sum_k n_k^n$	$\sum_k m_k^n$	$\|\sum_k m_k^n \boldsymbol{u}_k^n\|$	$\|\sum_k m_k^n \boldsymbol{E}_k^n\|$
3	$9.1.10^{-3}$	$2.5.10^{-3}$	$3.1.10^{-3}$	$7.4.10^{-3}$
10	$8.1.10^{-4}$	$1.2.10^{-4}$	$1.3.10^{-3}$	$3.4.10^{-3}$
100	$1.3.10^{-5}$	$2.0.10^{-7}$	$1.4.10^{-4}$	$3.4.10^{-4}$
OSM model				
100	$7.3.10^{-3}$	$3.2.10^{-3}$	$2.5.10^{-3}$	$2.2.10^{-3}$

Table 1 exhibits a convergence with a first order of accuracy for the velocity and the energy due to the constant reconstruction of the mean velocity and the variance in the section, whereas the order of accuracy is higher for the moments of order zero in the velocity [10]. However, the simulations are very accurate: with only 3 sections, the error of the TSM model is of the order of the OSM model with 100 sections. Reducing the number of sections is of paramount importance when going towards real cases that require very large computing grids as the CPU time scales with the number of sections for both transport and evaporation-drag steps. Moreover, for high evaporation rate, small size sections may limit the time step due to the CFL-like condition (see section 3.1). In the present case, for the same level of accuracy, the TSM model is found 780 faster than the OSM if the evaporation CFL limits the time step and 40 times faster if the transport CFL is limiting.

4.2. 2D Taylor-Green vortices

A numerical test is proposed to mimic the basic elements of the phenomena occurring in a real turbulent spray: droplets are put into motion by vortices, inducing trajectory crossings, while they are also evaporating. Figure 3.a shows the velocity field $\boldsymbol{u}_g = (u, v)$ of the carrier phase corresponding to the four contra-rotating Taylor-Green vortices used in the following numerical test, depending on the position $\boldsymbol{x} = (X, Y)$:

$$\begin{cases} u(Lx, Ly) &= u_0 \sin(2\pi x)\cos(2\pi y) \\ v(Lx, Ly) &= -u_0 \cos(2\pi x)\sin(2\pi y) \end{cases}$$

where L is the length and width of the domain and u_0 the maximum value of the velocity.

The initial spray velocity and energy is uniformly zero. The initial density distribution is provided by a cardinal sinus function while the initial size distribution is the same as in section 4.1. A key parameter of this test case is the Stokes number St, which corresponds to the non-dimensional drag relaxation time: $\mathrm{St} = \tau_p/\tau_g$ with $\tau_g = L/u_0$. From [6], we know that there exists a critical value $\mathrm{St}_c = 1/8\pi$ for which particles with $\mathrm{St} \geq \mathrm{St}_c$ are ejected from their original vortices. In the present case, we set $\mathrm{St}\,(S_{max}) = 32\mathrm{St}_c$, such that droplets larger than $S_{max}/32$

will be ejected and will generate trajectory crossings. The corresponding drag force coefficient is $1/\mathcal{A} = \pi/4\, S_{max}/\tau_g = 8.88285.10^{-9}\, m^2.s^{-1}$, since we chose $\tau_g = 1s$. With the given evaporation rate $K = 1.99.10^{-7}\, m^2.s^{-1}$, around half of the initial mass is evaporated during a simulation time $t = 1s$. The resulting size distribution at this time ensures that most droplets have a size S such that $St(S) > St_c$ so their trajectories will cross.

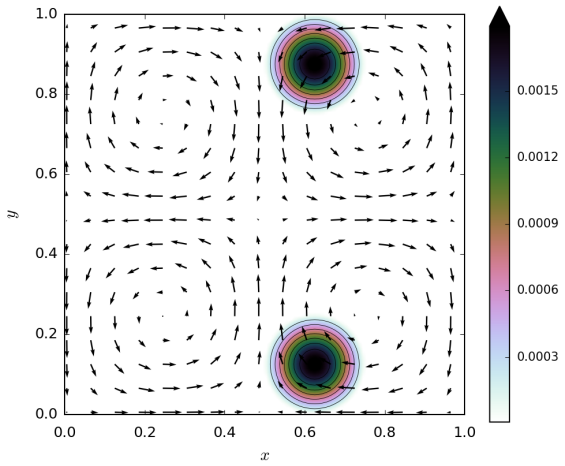

Figure 3: Carrier phase velocity field (Taylor-Green periodic vortices) and initial density contours.

In order to highlight the effect of the modeling approach, the TSM model with the anisotropic Gaussian (AG) velocity closure described in section 3 and noted AG-TSM is compared to two simpler models: the TSM model with a monokinetic velocity closure noted MK-TSM and the single section OSM model with the anisotropic Gaussian closure noted AG-mono, *mono* standing for monodisperse. Figure 4 shows the results for these three models at three successive instants. At $t = 0.5$, the MK-TSM and AG-TSM models give very similar results because there is no pressure effects so the AG-TSM model tends to the MK model. When droplet spots start to meet on the $y = 0$ line ($t \geq 0.75$), significant differences appear. With MK-TSM, all the mass is concentrated in a δ-shock on the meeting line. On the contrary, with AG-TSM, the creation of a velocity dispersion Σ_{22}, corresponding to a pression induced by the convergence of the two spots, prevents mass from accumulating on the centerline. The resulting distribution at $t = 1.1$ suggests a pattern corresponding to the two spots crossing whereas the solution for MK-TSM is clearly non-physical. As expected, the crossing pattern is also recovered by the AG-mono model but the solution clearly diverges from the 5-section AG-TSM as soon as the simulation starts. Indeed, the monodisperse description induces a different behavior in terms of total mass evaporation rate and drag acceleration. In the present case, it mainly results in a significant overestimation of the mass density compared to the AG-TSM model.

5. Conclusion

We proposed a hybrid model between sectional and moment methods, called AG-TSM. For each section of the size discretization, it combines a second order velocity moment method (with the anisotropic Gaussian closure) with the use of two pure size moments (with the affine by part reconstruction of the size NDF). To solve the corresponding system of equations with accuracy and robustness, a realizable numerical scheme was designed. The resulting method proved to be able to capture evaporation and drag with only a few sections. Compared to the single-size moment method, the same level of accuracy is achieved with the AG-TSM method using 40 or 800 times less CPU time, depending on whether transport or evaporation limits the time step, respectively. Moreover, the 2D Taylor-Green test case shows the importance of taking into account both the size and velocity dispersions to capture the fundamental phenomena of turbulent evaporating sprays.

The next step will be to evaluate in detail this promising model, as well as its extension to coalescence and break-up in order to tackle solid propulsion configurations. A second order realizable scheme for the transport will also be developed to increase the accuracy of the spatial resolution.

6. Acknowledgements

Aymeric Vié and Adam Larat are gratefully acknowledged for their help and discussions. This work is part of the NEXTFLAME project supported by the ANR and the FRAE through the grant ANR-13-BS09-0023-01.

References

[1] C. Berthon, M. Breuß, and M.O. Titeux. A relaxation scheme for the approximation of the pressureless Euler equations. *Numer. Methods for Partial Differential Equations*, 22(2):484–505, 2006.

[2] M. Boileau, C. Chalons, and M. Massot. Robust numerical coupling of pressure and pressureless gas dynamics equations for Eulerian spray DNS and LES. *SIAM J. Sci. Comput.*, 37(1):B79–B102, 2015.

[3] F. Bouchut. *Nonlinear stability of finite volume methods for hyperbolic conservation laws, and well-balanced schemes for sources*. Frontiers in Mathematics series, 2004.

[4] C. Chalons and F. Coquel. Navier-stokes equations with several independent pressure laws and explicit predictor-corrector schemes. *Numer. Math.*, 101(3):451–478, 2005.

[5] C. Chalons and J.-F. Coulombel. Relaxation approximation of the Euler equations. *J. Math. Anal. Appl.*, 348(2):872–893, 2008.

[6] S. de Chaisemartin. *Modèle eulériens et simulations numériques de brouillards de gouttes qui s'évaporent*. PhD thesis, Ecole Centrale Paris, 2009.

[7] O. Desjardins, R.O. Fox, and P. Villedieu. A quadrature-based moment method for dilute fluid-particle flows. *J. Comput. Phys.*, 227(4):2514 – 2539, 2008.

[8] F. Doisneau, F. Laurent, A. Murrone, J. Dupays, and M. Massot. Eulerian multi-fluid models for the simulation of dynamics and coalescence of particles in solid propellant combustion. *J. Comput. Phys.*, 234(0):230 – 262, 2013.

[9] F. Laurent. Numerical analysis of Eulerian multi-fluid models in the context of kinetic formulations for dilute evaporating sprays. *M2AN Math. Model. Numer. Anal.*, 40(3):431–468, 2006.

[10] F. Laurent, A. Sibra, and F. Doisneau. Two-size moment multi-fluid model: a robust and high-fidelity description of polydisperse moderately dense evaporating sprays. *Commun. Comput. Phys.*, pages 1–41, 2016. accepted, available online at https://hal.archives-ouvertes.fr/hal-01169730.

[11] C.D. Levermore and W.J. Morokoff. The Gaussian moment closure for gas dynamics. *SIAM J. Appl. Math.*, 59(1):72–96, 1998.

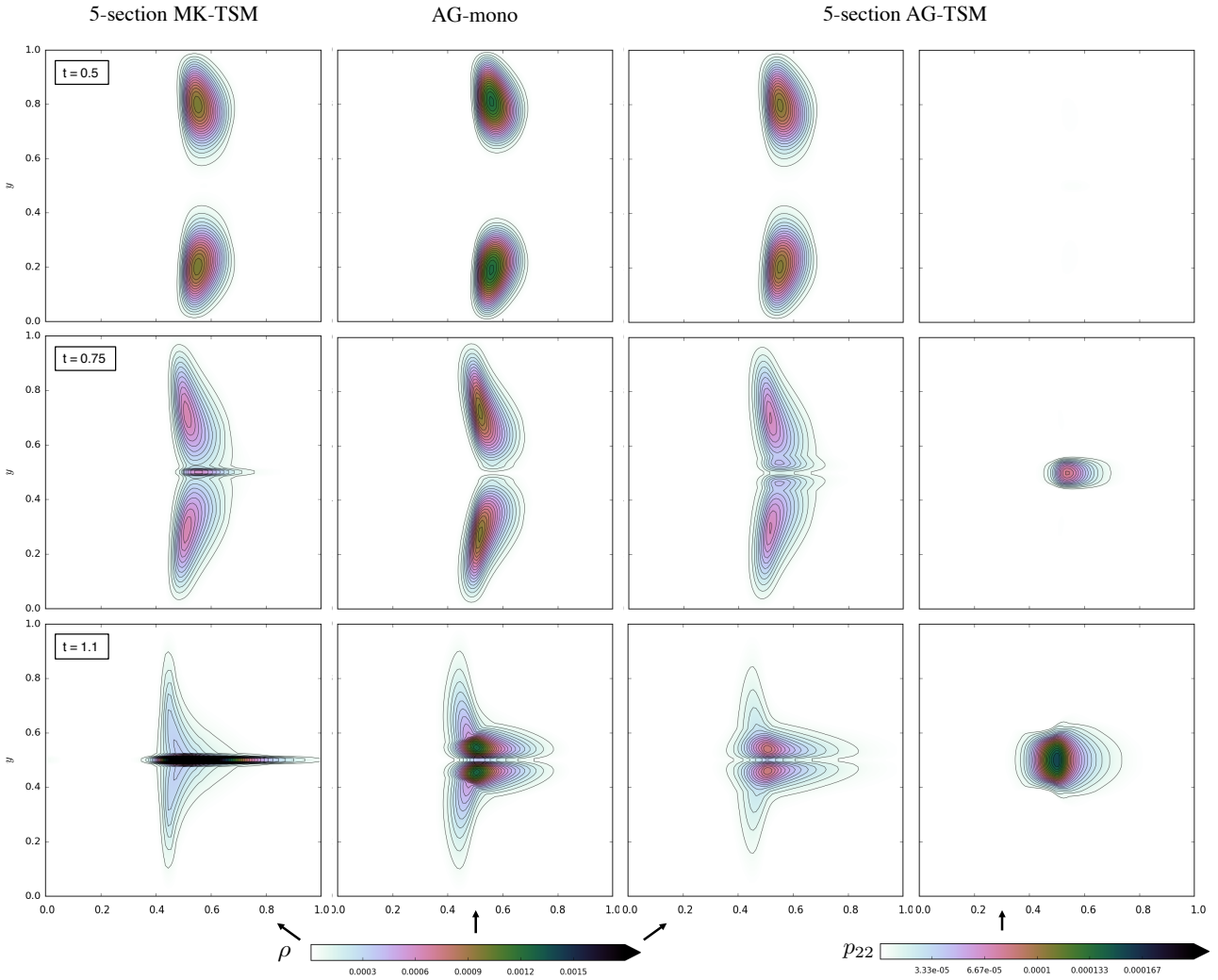

Figure 4: Three successive instants t of the simulation for three different models: polydisperse monokinetic (MK-TSM), monodisperse anisotropic Gaussian (AG-mono) and polydisperse anisotropic Gaussian (AG-TSM). Mass density distributions $\rho = \sum_k m_k$ are plotted for three models and the pressure in the y-direction $p_{22} = \sum_k m_k \Sigma_{k,22}$ is plotted for AG-TSM only.

[12] M. Sabat. *Modèles Eulériens et méthodes numériques pour la description des sprays polydispersés turbulents*. PhD thesis, Ecole Centrale Paris, France, 2016.

[13] M. Sabat, A. Vié, A. Larat, and M. Massot. Fully Eulerian simulation of 3D turbulent particle laden flow based on the Anisotropic Gaussian Closure. In *Proceedings of the International Conference on Multiphase Flows, Firenze, Italy*, pages 1–6, 2016.

[14] A. Sibra, J. Dupays, A. Murrone, F. Laurent, and M. Massot. Simulation of reactive polydisperse sprays strongly coupled to unsteady flows in solid rocket motors: Efficient strategy using eulerian multi-fluid methods. *J. Comput. Phys.*, 2016. accepted, available online at https://hal.archives-ouvertes.fr/hal-01063816.

[15] A. Vié, F. Doisneau, and M. Massot. On the Anisotropic Gaussian closure for the prediction of inertial-particle laden flows. *Commun. Comput. Phys.*, 17(1):1–46, 2015.

[16] F. A. Williams. Spray combustion and atomization. *Phys. Fluids*, 1:541–545, 1958.